warwick.ac.uk/lib-publications

Identification and Quantification of Ageing Mechanisms in Lithium-ion Batteries using the EIS technique

Carlos Pastor-Fernández,
W. Dhammika Widanage, James Marco
International Digital Laboratory
WMG, University of Warwick
Coventry, United Kingdom
c.pastor-fernandez@warwick.ac.uk
dhammika.widanalage@warwick.ac.uk, james.marco@warwick.ac.uk

Miguel-Ángel Gama-Valdez,
Gael. H. Chouchelamane
Jaguar Land Rover Limited
Gaydon, United Kingdom
mgamaval@jaguarlandrover.com
gchouch1@jaguarlandrover.com

Abstract—Ageing diagnosis in Lithium-ion batteries is essential to ensure their reliability and optimum performance over time. The Battery Management System (BMS) usually monitors battery ageing with the aid of two metrics: capacity and power fade. However, these metrics do not identify the main root causes of battery ageing. Using the Electrochemical Impedance Spectroscopy technique, this work proposes a novel method to identify and quantify ageing mechanisms over time. The method is applied to four parallelised Lithium-ion cells cycled with a constant driving profile for 500 cycles. As a result, Loss of Active Material (LAM) and Loss of Lithium Ions (LLI) were found to be the most pertinent ageing mechanisms over time for the four cells. Identification and quantification of ageing mechanisms will support novel battery lifetime control strategies within the BMS, so that potential failures during normal operation are prevented.

I. INTRODUCTION

State of Health (SoH) diagnosis represents a key measure to guarantee safety and lifetime optimised operation of Lithium-ion batteries (LIBs) in automotive applications [1]. The Battery Management System (BMS) usually quantifies SoH based on the decrease in capacity and increase in resistance, metrics that are directly related at a vehicle level to the range limit and power limit, respectively [1]. Such a definition of the SoH does not explain the root causes of battery degradation within a BMS, and thus identification and quantification of the ageing mechanisms are also needed [2]. Understanding the root causes of battery degradation will help the BMS to prevent potential failures such as internal short-circuit, overcharge or even thermal runaway. Ageing mechanisms are commonly classified into conductivity drops (Cond. loss), Loss of Lithium Ion (LLI) and Loss of Active Material (LAM) [3]. Incremental Capacity (IC) and Differential Voltage (DV) techniques have been extensively investigated to identify [2], [4] and quantify [3], [5] ageing mechanisms with the potential implementation within the BMS. Apart from this, previous research [6], [7] have demonstrated the potential of Electrochemical Impedance Spectroscopy (EIS) to identify ageing mechanisms offline in LIBs. In addition, some authors suggested the possibility of implementing this technique online [8], [9]. This study proposes an alternative technique to identify and quantify ageing mechanisms using EIS within the context of the BMS. This technique relates each of the resistors fitted from an Adapted Randles - Equivalent Circuit Model (AR-ECM) to conductivity losses, LLI or LAM. Using the EIS measurements, the AR-ECM is fitted based on the Non-Linear Least Squares (NLLS) algorithm. The capability to quantify the change of each ageing mechanism over time has the potential to achieve better real-time diagnosis performance of battery ageing within the BMS.

The structure of this work is divided as follows: Section II relates the background of EIS with the battery kinetic processes, describing the methodology and metrics employed to identify and quantify the most pertinent ageing mechanisms, Section III summarises the experimental investigation conducted for this work, Section IV shows the results obtained and finally, Section V draws the main outcomes of this study whilst Section VI outlines areas that could be further investigated.

II. METHODOLOGY

A. EIS technique

EIS represents a widely used experimental technique to gain a deeper insight into electrochemical processes of LIBs [10]. EIS results are usually represented by the inverse of Nyquist plots, which relates the imaginary (y-axis) and the real (x-axis) part of the impedance. The BMS often defines the internal impedance of the battery as the turning point at low frequency of the EIS plot [11], [12]. Fitting the Nyquist plots to a LIB ECM allows the battery kinetic processes to be modeled as illustrated in Figure 1A) and B).

The AR-ECM, which represents one of the most widely applied ECM in the literature [7], [14] - [16], is employed in this study. Figure 1B) illustrates that the AR-ECM is composed of a voltage source connected in series with a resistor, an inductor and resistor and Constant Phase Elements (CPEs)
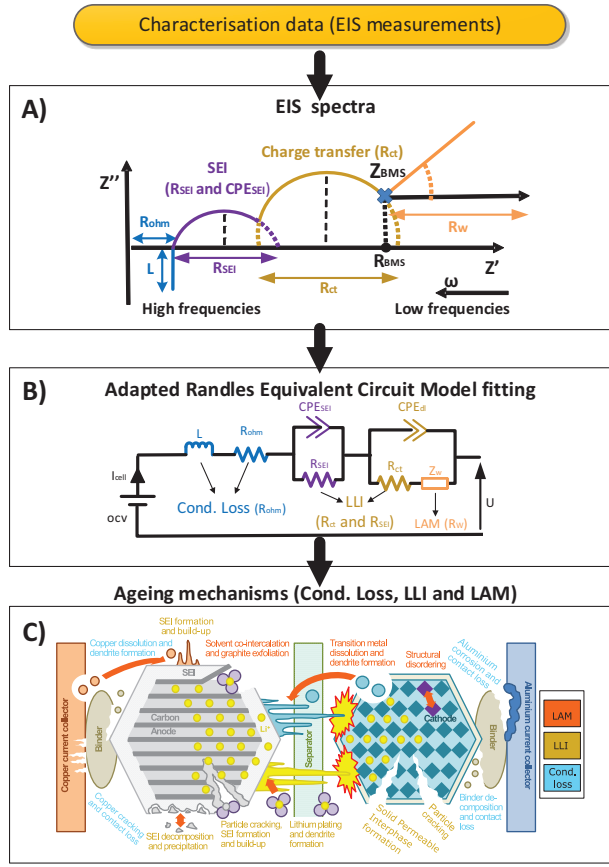
Fig. 1: Relationship between A) EIS spectrum, B) AR-ECM and C) ageing mechanisms (Bottom figure adapted from [13])

parallel branches. CPEs are often simplified by capacitors. In this case CPE's are employed to consider the porosity and tortuosity characteristics of the electrodes. The electrochemical significance of these elements as a function of the frequency, and how each relate to the different area of the EIS spectra is described below.

- **Open Circuit Voltage (OCV):** the OCV simulates the thermodynamic potential. The OCV is given in the form of a look-up table as a function of the SoC.
- **Loss of conductivity:** the ohmic resistance (R_{ohm}) accounts the voltage drops due to current collectors, binder, and electrode and electrolyte resistances [17]. The ohmic resistance R_{ohm} can be measured in the Nyquist plot as the point where the impedance spectrum crosses the real axis (zero imaginary component, refer to Figure 1A). In addition, an inductive behaviour in the current collectors is representative at high frequencies. The inductance L models this phenomenon, which in the Nyquist plot corresponds to the positive imaginary part of the impedance (see Figure 1A).
- **Passivation (SEI formation):** a passivation layer called

Solid Electrolyte Interface (SEI) that forms between the electrode and the electrolyte causes an irreversible decrease in capacity and increase in resistance [18]. During the first few cycles lithium is consumed in irreversible reactions at the anode. This lithiated carbon reacts with the electrolyte forming the SEI layer. The composition, thickness and morphology of the SEI changes over time causing subsequent degradation phenomena such as particle cracking. This phenomenon is characteristic at mid-frequencies and it is therefore related to the real impedance (horizontal distance) of first depressed semi-circle of the Nyquist plot. In the AR-ECM, a resistance called R_{SEI} is connected in parallel with a CPE element called CPE_{SEI} to model the SEI phenomenon [15], [19].

- **Charge-transfer and double layer capacitance:** the charge-transfer phenomenon represents the amount of electrochemical reactions to make possible intercalation and de-intercalation processes [20] (an electron is deposited onto an electrode site). The application of an electrical load to a cell will inherently accumulate charge carriers of different sign at the electrode/electrolyte interface. This charge accumulation across a short distance creates a capacitor-like effect (CPE_{dl}) called double-layer. The double-layer capacitance is proportional to the degree of porosity and tortuosity of the electrode. In the ECM, a resistance R_{ct} and a CPE_{dl} element connected in parallel models the charge-transfer and double layer phenomena, respectively. As for the first R-CPE branch (SEI) the Nyquist plot identifies the charge-transfer and double layer within its second depressed semicircle. R_{ct} is measured as the real part of the impedance (horizontal distance) of this mid-frequency depressed semicircle.
- **Diffusion:** diffusion is a phenomenon which includes the movement of charged and uncharged particles (mass transport) in order to balance concentration differences produced by the change in the electrochemical potential [20]. Diffusion takes place at low frequencies through the electrolyte, the electrode surface layers, and the active particles [17] and it is represented in the AR-ECM by the Warburg impedance. The Warburg resistance R_W represents the real part of the Z_W.

B. Identification of ageing mechanisms

This work proposes to track the change of the AR-ECM resistances (ohmic, SEI, charge-transfer and Warburg) as parameters to identify and quantify ageing mechanisms (Cond. loss, LLI and LAM) as illustrated in Figure 1. Each of the AR-ECM resistances can be related to an electrochemical phenomenon thus allowing to the most pertinent ageing mechanisms. In addition, the resistance itself represents an indicator of power fade which can be linked to the SoH. Table I relates each AR-ECM resistance to the most pertinent ageing mechanisms (Cond. loss, LLI and LAM) and their corresponding ageing root causes. In reality a single ageing mechanism underpins more than a single AR-ECM resistance. To simplify this

correlation, only the most significant ageing mechanism is related to each AR-ECM resistance.

TABLE I: Relationship between resistances of the AR-ECM with the most pertinent ageing mechanisms

R [Ω]	Ageing mechanism	Ageing mechanism root cause
R_{ohm}	Cond. loss	Copper dissolution dendrite formation. Copper cracking and contact loss. Aluminium corrosion and contact loss. Binder decomposition and contact loss.
R_{SEI} and R_{ct}	LLI	SEI formation and build-up. SEI decomposition and precipitation. Solid permeable interphase formation. Particle cracking, pore clogging and particle disconnection.
R_W	LAM	Solvent co-intercalation and graphite exfolation. Transition metal dissolution and dendrite formation. Structural disordering.

Ohmic resistance (R_{ohm}) accounts for the voltage drops due to current collector, binder, electrode and electrolyte electronic particles, which all are representative of Cond. loss ageing mechanism [28].

The formation of the SEI layer between the negative electrode and the electrolyte impedes the transition of the lithium ions from one electrode to the other. This will lead to LLI ageing mechanism since the amount of intercalated and de-intercalated lithium ions during charging and discharging is reduced [29]. Morphological changes in the structure of the electrodes (e.g. particle cracking) characteristic of LAM ageing mechanism can also lead to SEI growth [29]. This shows that LLI and LAM are interlinked.

Charge-transfer phenomenon represents the amount of electrochemical reactions to make possible intercalation and de-intercalation processes Section II-A. Thus, an increase of charge-transfer resistance R_{ct} implies that a lower amount of Li-ions are intercalated or de-intercalated [30]- [32]. This situation indicates that the increase of charge-transfer resistance can be treated as a measure of LLI ageing mechanism.

Large mass concentration differences between particles lead to structural transformations of the porous electrodes [18], [33], [34] allowing to correlate the increase of the Warburg resistance (real part of Z_W) to the LAM ageing mechanism.

C. Quantification of ageing mechanisms

Previous studies [3], [5] employ the capacity loss in percentage as a metric to quantify ageing mechanisms using IC/DV technique. In order to compare the results of this study with previous literature, the resistance loss in percentage is chosen as the parameter to identify and quantify ageing mechanisms. Equation 1, Equation 2 and Equation 3 compute the contribution of each ageing mechanism at each characterisation test $cht = n$ and $SoC = k$.

$$Cond.\ loss_{cont\ cht=n}^{SoC=k}(\%) = \frac{R_{ohm\ cht=n}^{SoC=k}(\%)}{R_{loss\ cht=n}^{SoC=k}(\%)} \cdot 100 \quad (1)$$

$$LLI_{cont\ cht=n}^{SoC=k}(\%) = \frac{R_{SEI\ cht=n}^{SoC=k}(\%) + R_{ct\ cht=n}^{SoC=k}(\%)}{R_{loss\ cht=n}^{SoC=k}(\%)} \cdot 100 \quad (2)$$

$$LAM_{cont\ cht=n}^{SoC=k}(\%) = \frac{R_{W\ cht=n}^{SoC=k}(\%)}{R_{loss\ cht=n}^{SoC=k}(\%)} \cdot 100 \quad (3)$$

For n = 1...11, k = 20%, 50% and 90%

Where Equation 4 computes the total loss of resistance in percentage over cycle number $R_{loss}(\%)$.

$$R_{loss\ cht=n}^{SoC=k}(\%) = \frac{R_{total\ cht=n}^{SoC=k}}{R_{total\ cht=1}^{SoC=k}} \cdot 100 \quad (4)$$

For n = 1...11, k = 20%, 50% and 90%

And Equation 5 computes the R_{total} as the sum of each resistance $R_{ohm}^{SoC=k}$, $R_{SEI}^{SoC=k}$, $R_{ct}^{SoC=k}$ and $R_W^{SoC=k}$.

$$R_{total\ cht=n}^{SoC=k} = R_{ohm\ cht=n}^{SoC=k} + R_{SEI\ cht=n}^{SoC=k} + R_{ct\ cht=n}^{SoC=k} + R_{W\ cht=n}^{SoC=k} \quad (5)$$

For n = 1...11, k = 20%, 50% and 90%

Then, Equation 6, Equation 7, Equation 8 and Equation 9 compute the importance of each resistance with respect to the total resistance R_{total}.

$$R_{ohm\ cht=n}^{SoC=k}(\%) = \frac{R_{ohm\ cht=n}^{SoC=k}}{R_{total\ cht=n}^{SoC=k}} \cdot 100 \quad (6)$$

$$R_{SEI\ cht=n}^{SoC=k}(\%) = \frac{R_{SEI\ cht=n}^{SoC=k}}{R_{total\ cht=n}^{SoC=k}} \cdot 100 \quad (7)$$

$$R_{ct\ cht=n}^{SoC=k}(\%) = \frac{R_{ct\ cht=n}^{SoC=k}}{R_{total\ cht=n}^{SoC=k}} \cdot 100 \quad (8)$$

$$R_{W\ cht=n}^{SoC=k}(\%) = \frac{R_{W\ cht=n}^{SoC=k}}{R_{total\ cht=n}^{SoC=k}} \cdot 100 \quad (9)$$

For n = 1...11, k = 20%, 50% and 90%

III. EXPERIMENTAL INVESTIGATION

To emulate the same conditions as in a commercially viable battery pack, four Nickel Cobalt Aluminium (NCA) Li-ion cells connected in parallel were cycled for 500 cycles until their End of Life (EoL). EoL corresponded to the state after which the battery reduces its capacity by 20% with respect to its Begin of Life (BoL) value. This definition is in agreement with several authors [21] - [25] and procedures [26], [27]. Undertaking the experimental investigation described in [11], each cell was aged initially by 0, 50, 100 and 150 cycles respectively before being connected in parallel to emulate an SoH imbalanced scenario. For simplicity this work is only focused on analysing the ageing mechanisms of the least aged

cell. The ageing mechanisms were similar for the rest of the cells. The ageing profile involved repeated cycles at constant 25°C of the following: a 1C discharge until the lower voltage limit was reached followed by Constant Current-Constant Voltage (CC-CV) charging. The CC phase involved charging the cell at C/2 to the end of charge voltage (4.2V). Then, the CV consisted on charging the cell until the current falls to C/20 (150mA). EIS tests in galvanostatic mode were performed on the newest cell individually between 4mHz and 100kHz at SoC=20%, SoC=50% and SoC=90%. SoC was adjusted based on the OCV value (OCV-SoC relationship). The EIS measurements were taken every 50 cycles using a Solartron modulab system (model 2100A), characterising the cell 11 times (n value) in total.

The EIS measurements were fitted employing the Zview software package, using the NLLS algorithm. The maximum error involved in each fitting measurement was of 10%. This fitting procedure could be implementable within the BMS in real-time scenarios [8], [9]. The required steps to perform such fitting process in the BMS are beyond of the scope of this study.

IV. RESULTS

A. Fitting results

Figure 2 illustrates the fitting results for R_{ohm}, R_{SEI}, R_{ct} and R_W. It can be seen that R_{ohm} and R_{SEI} remains almost constant over the number of cycles, whereas R_{ct} and R_W follow a linear increasing trend.

The change of R_{ohm} is independent of the SoC because R_{ohm} involves movement of electronic particles (voltage drops due to current collector, binder and electrode and electrolyte resistances) rather than ion particles.

R_{SEI} does not change significantly with respect to SoC, indicating that most of the SEI dynamics are represented by the R_{ct}. This result indicates that the SEI R-CPE parallel branch could be removed, simplifying the ECM.

For SoC 20% the value of R_{ct} and R_W is larger than at SoC 50% and SoC 90%. This result is explained based on the fact that the rate of the intercalation and de-intercalation of lithium-ions (Li-ions) between the electrodes depends on the amount of Li-ion concentrated at the surface of the electrodes, which is a function of the SoC (refer to Nernst equation) [20]. The concentration of Li-ions is higher at SoC 20% than at 50% and 90% because the active surface area of the cathode (between 0.5-5m²/g) in general is lower than the anode (between 3-15m²/g) [35]. For this case (charging event, the order of the EIS measurements taken was SoC 20%, 50% and 90%) the ions move from the cathode (low SoC) to the anode (high SoC). Then, the larger concentration of Li-ions implies the R_{BMS} is larger at SoC 20% than at 50% and 90%.

This result is in agreement with other studies [36] - [40] which evaluated the change of cell internal resistance with respect to the SoC.
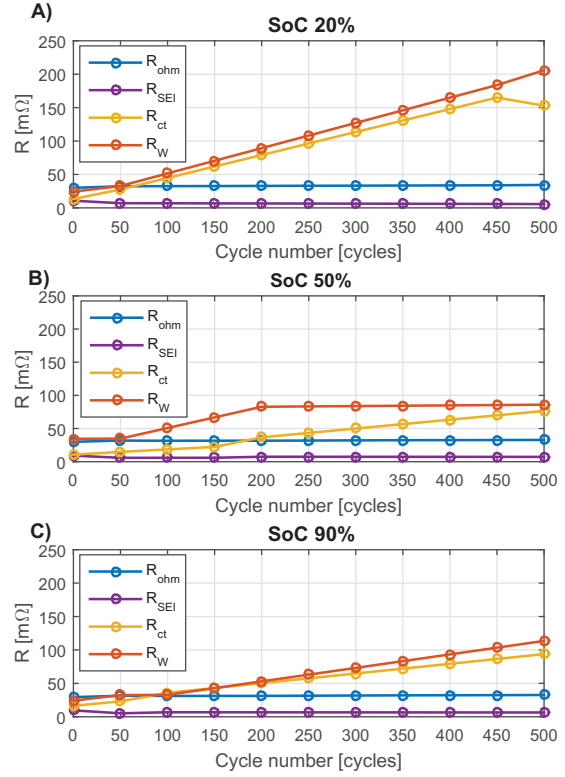

Fig. 2: Fitting results of R_{ohm}, R_{SEI}, R_{ct} and R_W at A) SoC 20%, B) SoC 50% and C) SoC 90% over number of cycles

B. Identification and quantification of ageing mechanisms

Using Equation 1, Equation 2 and Equation 3, the contribution of each ageing mechanism is computed with respect to the total loss of resistance. Figure 3 outlines that the magnitude of R_{loss} for each ageing mechanism follows a linear trend based on the growth of the fitting resistances. It can be seen that LLI and LAM represent the most pertinent ageing mechanisms over cycle number independently on the SoC due to the high magnitude value of R_{ct} and R_W (refer to Figure 2). The Cond. loss grows slightly with cycle number as a result of the low magnitude value of R_{ohm} (refer to Figure 2). The increase in loss of resistance ($R_{loss}(\%)$) over cycle number is larger for 20% SoC than for 50% and 90% due to a larger concentration of Li-ions as explained in Section IV-A. In overall, this result agree with the outcome obtained in previous work [3], [5], where the IC and DV analysis were employed to quantify LLI and LAM based on the capacity fade. For a similar cell chemistry and testing conditions they conclude that LAM and LLI represent the most pertinent ageing mechanisms. As a difference with respect to the results here presented, LAM is reported to increase exponentially over time and LLI to decrease linearly. These trends were not identified within this

work, where LAM and LLI increases linearly. The reasons to explain this difference can be very diverse. For instance, the type of technique (IC/DV instead of EIS) or the parameter used (capacity instead of resistance) are different.
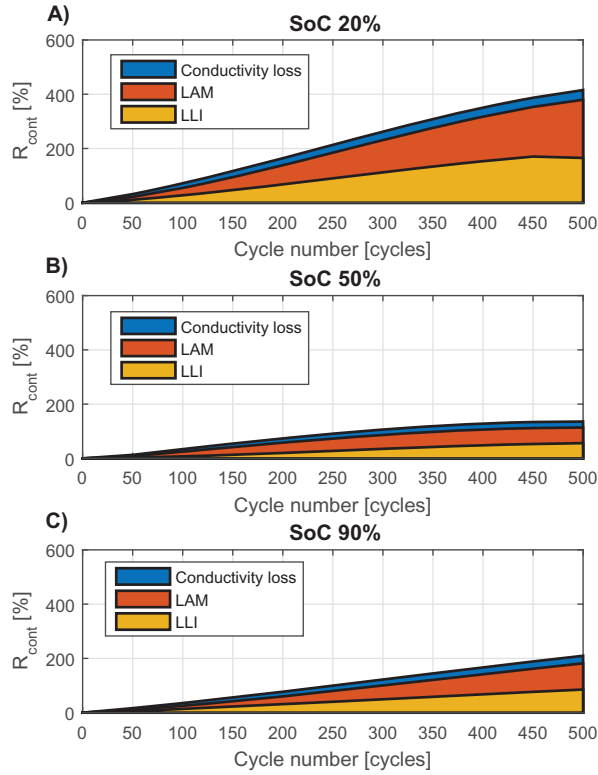

Fig. 3: Contribution to battery degradation of each ageing mechanism at A) SoC 20%, B) SoC 50% and C) SoC 90% over number of cycles

V. CONCLUSIONS

For a particular experimental investigation, this study proposes a method to identify and quantify ageing mechanisms using EIS. It was demonstrated that LAM and LLI contribute more to battery degradation than conductivity losses. This contribution is more enhanced at SoC 20% than at 50% and 90%. This method could be implementable in the future within the BMS for real-time applications. The outcome of this technique would help to understand the root causes of battery degradation over time without restrictions on cell chemistry, battery sizes and geometries, cell designs and operating conditions. Quantifying the root causes of battery degradation will give the capability to the BMS to prevent battery failures during normal operation.

VI. FURTHER WORK

Further work includes implementing this technique on-board within the BMS, so that the BMS would understand the causality of degradation over time (Cond. loss, LAM or LLI). In addition, the electrochemical insights obtained could be validated using post-mortem analysis such as Scanning Electron Microscopy (SEM), Energy Dispersive Spectrometry (EDS) or X-Ray Diffractometry (XRD) [41]. These in-situ techniques can identify more accurately the ageing mechanisms in LIBs.

ACKNOWLEDGMENTS

NOMENCLATURE

Symbols

cht	characterisation test
ct	charge-transfer
$cont$	contribution
dl	double layer
k	SoC (20%, 50% or 90%)
n	number of characterisation test
mag	Magnitude
$Ncycle$	Number of cycles
Ohm	Ohmic
W	Warburg

REFERENCES

[1] P. Weicker, A systems approach to Lithium-Ion mattery management. Artech House, 2014.

[2] X. Han, M. Ouyang, L. Lu, J. Li, Y. Zheng, and Z. Li, A comparative study of commercial lithium ion battery cycle life in electrical vehicle: Aging mechanism identification, J. Power Sources, vol. 251, pp. 3854, Apr. 2014.

[3] M. Dubarry, C. Truchot, and B. Y. Liaw, Synthesize battery degradation modes via a diagnostic and prognostic model, J. Power Sources, vol. 219, pp. 204216, 2012.

[4] M. Dubarry, B. Y. Liaw, M.-S. Chen, S.-S. Chyan, K.-C. Han, W.-T. Sie, and S.-H. Wu, Identifying battery aging mechanisms in large format Li ion cells, J. Power Sources, vol. 196, no. 7, pp. 34203425, Apr. 2011.

[5] B. Y. Liaw, A. Devie, and M. Dubarry, The Value of Battery Diagnostics and Prognostics.

[6] Y. Zhang and C.-Y. Wang, Cycle-Life Characterization of Automotive Lithium-Ion Batteries with LiNiO2 Cathode, J. Electrochem. Soc. , vol. 156 , no. 7 , pp. A527A535, Jul. 2009.

[7] P. Aurora, N. Ramaswamy, and T. Han, Electrochemical Impedance Spectroscopic Analysis of Lithium-ion Battery Aging Mechanisms, ECS Trans., vol. 147, no. 2005, p. 2013, 2010.

[8] J. Remmlinger, M. Buchholz, M. Meiler, P. Bernreuter, and K. Dietmayer, State-of-health monitoring of lithium-ion batteries in electric vehicles by on-board internal resistance estimation, J. Power Sources, vol. 196, no. 12, pp. 53575363, Jun. 2011.

[9] D. A. Howey, P. D. Mitcheson, V. Yufit, G. J. Offer and N. P. Brandon, Online Measurement of Battery Impedance Using Motor Controller Excitation, in IEEE Transactions on Vehicular Technology, vol. 63, no. 6, pp. 2557-2566, July 2014.

[10] E. Barsoukov, J.R. Macdonald, Impedance Spectroscopy, Theory, Experiment, and Applications, second ed., John Wiley Sons, New Jersey, 2005

[11] T. Bruen, J. Marco, and M. Gama, Current Variation in Parallelized Energy Storage Systems, Vehicle Power and Propulsion Conference (VPPC), 2014 IEEE. pp. 16, 2014.

[12] D. Andre, M. Meiler, K. Steiner, H. Walz, T. Soczka-Guth, and D. U. Sauer, Characterization of high-power lithium-ion batteries by electrochemical impedance spectroscopy. II: Modelling, J. Power Sources, vol. 196, no. 12, pp. 53495356, Jun. 2011.

[13] C. R. Birkl, Degradation mechanisms. [Online]. Available: http://epg.eng.ox.ac.uk/content/degradation-lithium-ion-batteries. [Accessed: 12-Jan-2016].

[14] T. K. Dong, A. Kirchev, F. Mattera, J. Kowal, and Y. Bultel, Dynamic Modeling of Li-Ion Batteries Using an Equivalent Electrical Circuit, J. Electrochem. Soc. , vol. 158 , no. 3 , pp. A326A336, Mar. 2011.

[15] R. Al-Nazer and V. Cattin, A new optimization algorithm for a Li-Ion battery equivalent electrical circuit identification, 9th Int. Conf. Model. Optim. Simul. - MOSIM12, no. Mosim, 2012.

[16] J. P. Schmidt, T. Chrobak, M. Ender, J. Illig, D. Klotz, and E. Ivers-Tiffe, Studies on LiFePO4 as cathode material using impedance spectroscopy, J. Power Sources, vol. 196, no. 12, pp. 53425348, Jun. 2011

[17] D. P. Abraham, S. D. Poppen, A. N. Jansen, J. Liu, and D. W. Dees, Application of a lithiumtin reference electrode to determine electrode contributions to impedance rise in high-power lithium-ion cells, Electrochim. Acta, vol. 49, no. 26, pp. 47634775, Oct. 2004.

[18] J. Vetter, P. Novk, M. R. Wagner, C. Veit, K.-C. Mller, J. O. Besenhard, M. Winter, M. Wohlfahrt-Mehrens, C. Vogler, and A. Hammouche, Ageing mechanisms in lithium-ion batteries, J. Power Sources, vol. 147, no. 12, pp. 269281, Sep. 2005.

[19] H. Dong, X. Jin, Y. Lou, and C. Wang, Lithium-ion battery state of health monitoring and remaining useful life prediction based on support vector regression-particle filter, J. Power Sources, vol. 271, no. 0, pp. 114123, 2014.

[20] H. J. Bergveld, Battery Management Systems Design by Modelling, PhD Thesis, Twente University, 2001.

[21] M. Ecker, J. B. Gerschler, J. Vogel, S. Kbitz, F. Hust, P. Dechent, and D. U. Sauer, Development of a lifetime prediction model for lithium-ion batteries based on extended accelerated aging test data, J. Power Sources, vol. 215, no. 0, pp. 248257, 2012.

[22] A. Farmann, W. Waag, A. Marongiu, and D. U. Sauer, Critical review of on-board capacity estimation techniques for lithium-ion batteries in electric and hybrid electric vehicles, J. Power Sources, vol. 281, pp. 114130, Jan. 2015.

[23] D. Andre, C. Appel, T. Soczka-Guth, and D. U. Sauer, Advanced mathematical methods of SOC and SOH estimation for lithium-ion batteries, J. Power Sources, vol. 224, no. 0, pp. 2027, 2013.

[24] A. Nuhic, T. Terzimehic, T. Soczka-Guth, M. Buchholz, and K. Dietmayer, Health diagnosis and remaining useful life prognostics of lithiumion batteries using data-driven methods, J. Power Sources, vol. 239, no. 0, pp. 680688, 2013.

[25] Berecibar, M.; Omar, N.; Garmendia, M.; Dubarry, M.; Villarreal, I.; Van den Bossche, P.; Van Mierlo, Joeri, SOH Estimation and Prediction for NMC Cells Based on Degradation Mechanism Detection, in Vehicle Power and Propulsion Conference (VPPC), 2015 IEEE, vol., no., pp.1-6, 19-22 Oct. 2015

[26] INL/EXT-07e12536, Rev 0, Battery Test Manual for Plug-in Hybrid Electric Vehicles, U.S. Department of Energy Vehicle Technologies Program, March 2008.

[27] USABC, Electric Vehicle Battery Test Procedures - Rev. 2, United States Adv. Batter. Consort., no. January, 1996.

[28] A. Barai, G. H. Chouchelamane, Y. Guo, A. McGordon, and P. Jennings, A study on the impact of lithium-ion cell relaxation on electrochemical impedance spectroscopy, J. Power Sources, vol. 280, pp. 7480, Apr. 2015.

[29] A. J. Smith, J. C. Burns, D. Xiong, and J. R. Dahn, Interpreting High Precision Coulometry Results on Li-ion Cells, J. Electrochem. Soc., vol. 158, no. 10, pp. A1136A1142, 2011.

[30] H. Liu, Q. Cao, L. J. Fu, C. Li, Y. P. Wu, and H. Q. Wu, Doping effects of zinc on LiFePO4 cathode material for lithium ion batteries, Electrochem. commun., vol. 8, no. 10, pp. 15531557, Oct. 2006.

[31] P. Guo, H. Song, and X. Chen, Electrochemical performance of graphene nanosheets as anode material for lithium-ion batteries, Electrochem. commun., vol. 11, no. 6, pp. 13201324, Jun. 2009.

[32] T. R. Jow, J. Allen, M. Marx, K. Nechev, B. Deveney, and S. Rickman, Electrolytes, SEI and Charge Discharge Kinetics in Li-Ion Batteries, ECS Trans., vol. 25, no. 36, p. 312, 2010.

[33] M. Broussely, P. Biensan, F. Bonhomme, P. Blanchard, S. Herreyre, K. Nechev, and R. J. Staniewicz, Main aging mechanisms in Li ion batteries, J. Power Sources, vol. 146, no. 12, pp. 9096, 2005.

[34] A. Barr, B. Deguilhem, S. Grolleau, M. Grard, F. Suard, and D. Riu, A review on lithium-ion battery ageing mechanisms and estimations for automotive applications, J. Power Sources, vol. 241, pp. 680689, Nov. 2013.

[35] M. V Reddy, G. V Subbarao, and B. V. R. Chowdari, Cathode and anode materials for Lithium Ion Batteries.

[36] D. I. Stroe, M. Swierczynski, a I. Stan, V. Knap, R. Teodorescu, and S. J. Andreasen, Diagnosis of lithium-ion batteries state-of-health based on electrochemical impedance spectroscopy technique, Energy Convers. Congr. Expo. (ECCE), 2014 IEEE, pp. 45764582, 2014.

[37] W. Waag, S. Kbitz, and D. U. Sauer, Experimental investigation of the lithium-ion battery impedance characteristic at various conditions and aging states and its influence on the application, Appl. Energy, vol. 102, pp. 885897, Feb. 2013.

[38] D. Andre, M. Meiler, K. Steiner, C. Wimmer, T. Soczka-Guth, and D. U. Sauer, Characterization of high-power lithium-ion batteries by electrochemical impedance spectroscopy. I. Experimental investigation, J. Power Sources, vol. 196, no. 12, pp. 53345341, Jun. 2011.

[39] S. Rodrigues, N. Munichandraiah, and a. K. Shukla, AC impedance and state-of-charge analysis of a sealed lithium-ion rechargeable battery, J. Solid State Electrochem., vol. 3, no. 78, pp. 397405, 1999.

[40] B. V. Ratnakumar, M. C. Smart, L. D. Whitcanack, and R. C. Ewell, The impedance characteristics of Mars Exploration Rover Li-ion batteries, J. Power Sources, vol. 159, no. 2, pp. 14281439, Sep. 2006.

[41] E. Sarasketa-Zabala, F. Aguesse, I. Villarreal, L. M. Rodriguez-Martinez, C. M. Lpez, and P. Kubiak, Understanding Lithium Inventory Loss and Sudden Performance Fade in Cylindrical Cells during Cycling with Deep-Discharge Steps, J. Phys. Chem. C, vol. 119, no. 2, pp. 896906, 2015.